# Experimental and Numerical Study on a Hall Thruster Insulator Erosion

**IEPC-2011-078**

*Presented at the 32nd International Electric Propulsion Conference,*
*Wiesbaden • Germany*
*September 11 – 15, 2011*

Shinatora Cho[1]
*The University of Tokyo, Tokyo, 113-8656, Japan*

Shigeru Yokota[2]
*Nagoya University, Nagoya, 464-8603, Japan*

*and*

Ryotaro Kaneko[3], Kimiya Komurasaki[4], and Yoshihiro Arakawa[5]
*The University of Tokyo, Tokyo, 113-8656, Japan*

**Insulator erosion of a SPT-type Hall thruster was evaluated by both numerical analysis and measurement. Ion wall loss and channel wall reduction rate was computed by using 2D3V Fully Kinetic Particle-In-Cell Direct Simulation Monte Carlo model. Electrons are treated as particle for wall sheath modeling. In order to avoid the use of artificial electric permittivity, the time accuracy of the field solver was improved, and partially implicit method was introduced. The simulated wall reduction rate was compared with the measurement result of Multilayer Coating Method, which is an accelerated erosion measurement method using small multilayer coated chips as sensor of erosion detection.**

## Nomenclature

| | | |
|---|---|---|
| $m$ | = | mass |
| $q$ | = | charge |
| $\boldsymbol{E}$ | = | electric field |
| $\boldsymbol{v}$ | = | velocity |
| $\boldsymbol{B}$ | = | magnetic flux density |
| $\varepsilon$ | = | permittivity |
| $\rho$ | = | charge density |
| $\Delta t$ | = | time step |
| $\boldsymbol{j}$ | = | current density |
| $\nu$ | = | collision frequency |

[1] Ph.D. Candidate, Department of Aeronautics and Astronautics, cho@al.t.u-tokyo.ac.jp.
[2] Assistant Professor, Department of Aerospace Engineering, yokota@nuae.nagoya-u.ac.jp.
[3] Graduate Student, Department of Aeronautics and Astronautics, kaneko@al.t.u-tokyo.ac.jp.
[4] Professor, Department of Advanced Energy, komurasaki@k.u-tokyo.ac.jp.
[5] Professor, Department of Aeronautics and Astronautics, arakawa@al.t.u-tokyo.ac.jp.

$e$ = elementary charge
$n_e$ = electron density
$\theta$ = parameter
$\omega_p$ = plasma frequency
$\phi$ = potential
$\boldsymbol{n}$ = normal unit vector
$n_e$ = electron density
$\gamma$ = volume fraction
$V$ = volume
$Y$ = sputtering yield
$E$ = ion energy
$E_{\text{th}}$ = threshold ion energy
$A, B$ = coefficient

## I. Introduction

The lifetime performance of a Hall thruster is highly important for its further application to space missions. The primary lifetime-limiting factor of Hall thrusters is the insulator erosion caused by ion bombardment inside the discharge channel. Various experimental[1-3] and numerical[4-6] erosion studies were conducted in different institutes. Recent studies even indicate that the erosion-free Hall thruster can be realized. [6-7] However, still the strategy and mechanism of erosion reduction is not fully understood mainly because of the very costly lifetime endurance test[7-9]. Therefore, further development of accelerated erosion measurement method and self-consistent numerical model is necessary to uncover the physical background. As the first step of lifetime evaluation system without relying on long-time endurance tests, both numerical and experimental study was conducted.

Most of the numerical works use Hybrid Particle-In-Cell (PIC) model because of its moderate description accuracy and low computational cost. [4-5] However, Hybrid-PIC models assume quasi-neutrality throughout the calculation domain, which means that the self-consistent wall sheath prediction is impossible. Therefore, the Fully Kinetic PIC Direct Simulation Monte Carlo (DSMC) model[10-11] was selected. It is well known that the conventional fully kinetic model is computationally expensive, and requires acceleration technique of artificial mass ratio and artificial permittivity, which can cause unrecoverable change of physics. To improve these drawbacks, we introduced partially implicit field solver in this study, [12] and shown that it is possible to conduct simulation by acceptable computational cost *without* using artificial permittivity.

The result of numerical analysis was compared with that of the multilayer coating measurement[13] in order to compensate for the shortage of Boron Nitride (BN) sputtering yield data for low energy xenon ion impact. The Multilayer Coating Method is a new accelerated erosion measurement method developed in the University of Tokyo. It measures the wall reduction rate by using small multilayer coated chips as sensor of erosion detection, which enables both direct and low-cost repetitive measurement.

## II. Models

### A. Fully Kinetic Model

Figure 1 shows the flow chart of 2D3V fully kinetic PIC model. Finite Volume Method was used for the field solver, and its detail will be described in the next section.

As for the simulation of particle trajectory, the equation of motion in cylindrical coordinate can be written as equation 1, and was solved by fourth order Runge-Kutta method.

$$m\dot{\boldsymbol{v}} = q(\boldsymbol{E} + \boldsymbol{v} \times \boldsymbol{B}) \quad (1)$$

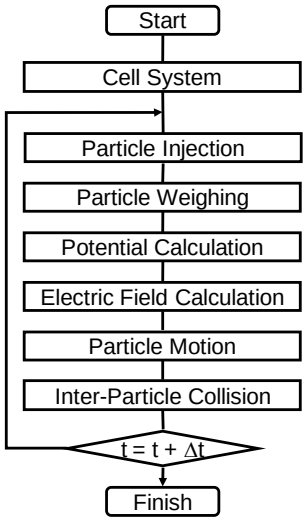


**Figure 1. Calculation flow chart.**

For modeling of inter-particle collision, we used DSMC method. The Bohm diffusion was implemented in terms of virtual scattering collision between neutral and electron.[11]

**B. Field Solver**

Potential solver was improved in order to realize fully kinetic simulation without artificially manipulating permittivity by using the method originates from Ref. 12. Conventionally, the electric field and potential were obtained by solving following Gauss's law.

$$\boldsymbol{\nabla} \cdot (\varepsilon \boldsymbol{E}^{m+1}) = \rho^m \tag{2}$$

Where $\varepsilon$ is permittivity, $\boldsymbol{E}$ is electric field, $\rho$ is charge density, and the superscripts denote the time step. Equation 2 means that the field of next time step is calculated by the charge distribution of current step with 0th order time accuracy. Instead, 1st order accurate method can be obtained by using the conservation of charge, or taking the divergence of Ampere's law.

$$\boldsymbol{\nabla} \cdot (\varepsilon \boldsymbol{E}^{m+1}) = \boldsymbol{\nabla} \cdot (\varepsilon \boldsymbol{E}^{m}) + \frac{\partial}{\partial t}[\boldsymbol{\nabla} \cdot (\varepsilon \boldsymbol{E}^{m})]\Delta t = \rho^m - \boldsymbol{\nabla} \cdot \boldsymbol{j}^m \Delta t \tag{3}$$

Where $\boldsymbol{j}$ is the net current density, and $\Delta t$ is the time step. If we make the method partially implicit, then the Eq. 3 can be rewritten as follows.

$$\boldsymbol{\nabla} \cdot (\varepsilon \boldsymbol{E}^{m+1}) = \rho^m - \boldsymbol{\nabla} \cdot \boldsymbol{j}^{m+1} \Delta t \tag{4}$$

$$\boldsymbol{j}^{m+1} \cong \boldsymbol{j}_i^m + (1 - \nu_{en}^m \Delta t)\boldsymbol{j}_e^m + \frac{e^2 n_e^m \Delta t}{m_e}(\theta \boldsymbol{E}^{m+1} + (1-\theta)\boldsymbol{E}^m) + \frac{e\Delta t}{m_e}(\boldsymbol{j}_e^m \times \boldsymbol{B}) \tag{5}$$

Where $\nu_{en}^m$ is electron-neutral collision frequency, $n_e$ is electron density, $\boldsymbol{B}$ is magnetic flux density, and $\theta$ is implicit parameter ($0 \le \theta \le 1$). The time variation of ion current is small and was neglected. Although it is costly to solve Eq. 4 and Eq. 5 directly, if we assume Eq. 6 is valid that the gradient of electron density is relatively small, then the system will be simplified to be Eq. 7.

$$\boldsymbol{\nabla} \cdot (n_e^m \boldsymbol{E}^{m+1}) \cong n_e^m \boldsymbol{\nabla} \cdot \boldsymbol{E}^{m+1} \tag{6}$$

$$\boldsymbol{\nabla} \cdot (\varepsilon \boldsymbol{E}^{m+1}) \cong \frac{1}{1+\theta(\omega_p \Delta t)^2}\left\{\rho^m - \boldsymbol{\nabla} \cdot \left[\boldsymbol{j}_i^m + (1 - \nu_{en}^m \Delta t)\boldsymbol{j}_e^m + \frac{e^2 n_e^m \Delta t}{m_e}(1-\theta)\boldsymbol{E}^m + \frac{e\Delta t}{m_e}(\boldsymbol{j}_e^m \times \boldsymbol{B})\right]\Delta t\right\} \tag{7}$$

Where $\omega_p$ is plasma frequency. In Eq. 7, obviously, fluctuation on the order of plasma frequency will be time-averaged and smoothed away. Practically, with the use of artificial mass ratio, $(\omega_p \Delta t)^2$ reduce to maximum around 0.2 that the improvement of field solver is supposed to be mainly contributed by the improvement of time accuracy.

In this study, we applied Finite Volume Method to Eq. 8 and Eq. 9 with $\theta = 0.5$ for obtaining the potential and electric field.

$$\iint \varepsilon \boldsymbol{\nabla} \phi^{\mathrm{m+1}} \cdot \boldsymbol{n}\mathrm{dS} = \frac{1}{1+\theta(\omega_p \Delta t)^2}\left\{-\iiint \rho^m \,\mathrm{dV} + \iint \left[\boldsymbol{j}_i^m + (1 - \nu_e^m \Delta t)\boldsymbol{j}_e^m + \frac{e^2 n_e \Delta t}{m_e}(1-\theta)\boldsymbol{E}^m + \frac{e\Delta t}{m_e}(\boldsymbol{j}_e^m \times \boldsymbol{B})\right]\Delta t \cdot \boldsymbol{n}\mathrm{dS}\right\} \tag{8}$$

$$\boldsymbol{E} = -\boldsymbol{\nabla}\phi \tag{9}$$

Because the field inside the insulator wall was also solved in this study, the electric permittivity $\varepsilon$ is not always equal to the vacuum permittivity, and can be written as

$$\varepsilon = [\gamma + (1-\gamma)\varepsilon_{BN}]\varepsilon_0 \tag{10}$$

$$\gamma = \frac{V_{vaccum}}{V_{vaccum}+V_{BN}} \tag{11}$$

Where $\gamma$ is volume fraction of the cell, and $V$ represents the volume.

### C. Numerical Assumptions

Although the artificial permittivity was removed from the model to avoid summing up nonlinear correction effects, still several numerical assumptions were necessary for the simulation. The all used assumptions are shown by Table 1.

The artificial mass ratio[10-11] was introduced that the mass of electron was artificially increased by 2,500 times in this study. In addition, the concept of super particle was used, and one simulation particle represents $5.0\times10^7$ real particles. For typical condition, there exist about 100 particles per cell in average for each species (except doubly charged ion).

Because the code ignores azimuthal electric field, the Bohm diffusion was introduced with the coefficient of 1/16 to compensate for the reduced electron mobility across the magnetic field.[11]

The magnetic field induced by the plasma is considered to be negligible. The magnetic flux density distribution was calculated in advance by using free software FEMM.

As for the particle species and collisions, four kinds of dominant particles; ions, doubly charged ions, electrons, and neutrals were simulated, and corresponding collisions of ionization, Xe – $e^-$ excitation, and Xe – $e^-$ scattering were modeled. The fraction of triply or higher charged ions was considered to be small, and was neglected along with the corresponding collisions.

The computational time step was $5.0\times10^{-10}$ s, and spatial resolution was $2.0\times10^{-4}$ m. With these conditions, the typical computational cost is about 15 hours per 0.1 ms simulation with single core 3.3 GHz CPU, which is considered to be acceptable.

### D. Hall Thruster

The geometry of SPT-type Hall thruster of the University of Tokyo was modeled in this study. This thruster was selected because all of the specifications and data of various performance and lifetime study are available[13-14]. Figure 2 shows the schematic of the thruster.

**Table 1. Numerical assumptions.**

| Assumptions | status |
|---|---|
| Artificial mass ratio | 2,500 times multiplied electron mass |
| Artificial permittivity | NOT used |
| Super particle | $5.0\times10^7$ |
| Time step | $5.0\times10^{-10}$ s |
| Spatial Resolution | $2.0\times10^{-4}$ m |
| Bohm coefficient | 1/16 |
| Magnetic field | Constant |
| Particles | e , Xe, $Xe^+$, $Xe^{++}$ |
| Collision | $e^-$–Xe elastic scattering, $e^-$–Xe ionization, e –Xe excitation |

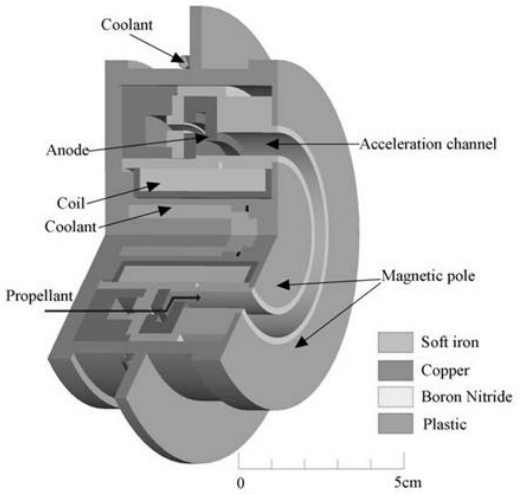


**Figure 2. Schematic of UT SPT-type Hall thruster.** *Middle size Hall thruster developed in the University of Tokyo with outer channel diameter 62 mm, inner channel diameter 48 mm, and channel length 21 mm.*

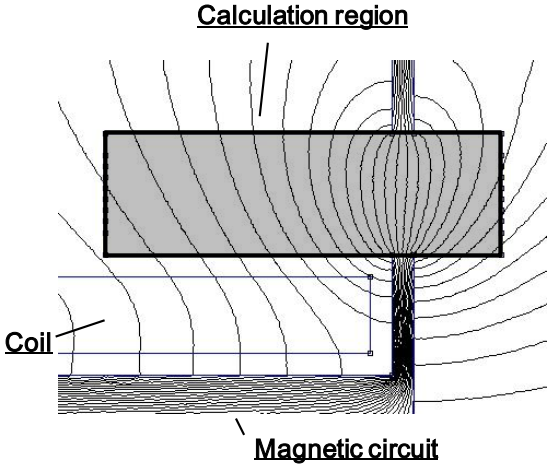


**Figure 3. Magnetic field configuration.** *The magnetic field was considered to be stable during the discharge, and was calculated by free software FEMM in advance.*

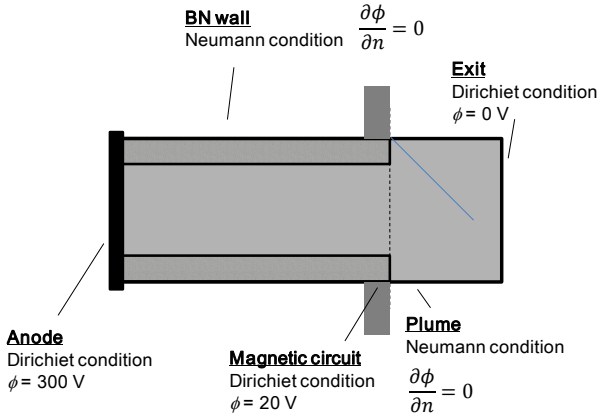


**Figure 4. Boundary conditions for field solver.**
*The electric field within the ceramic wall was directly calculated.*

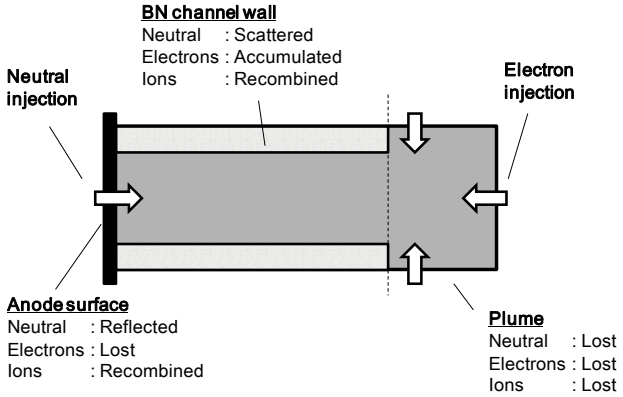


**Figure 5. Boundary conditions for Particles.**

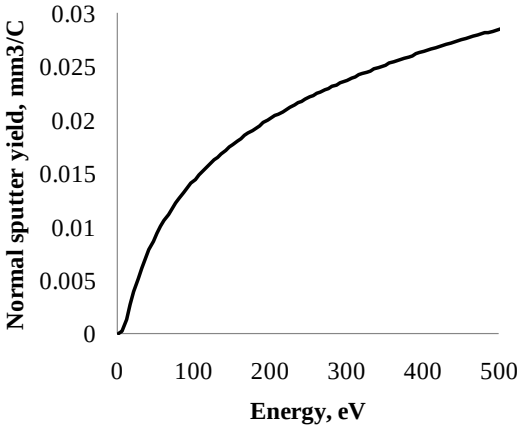


**Figure 6. Normal sputter yield model.**

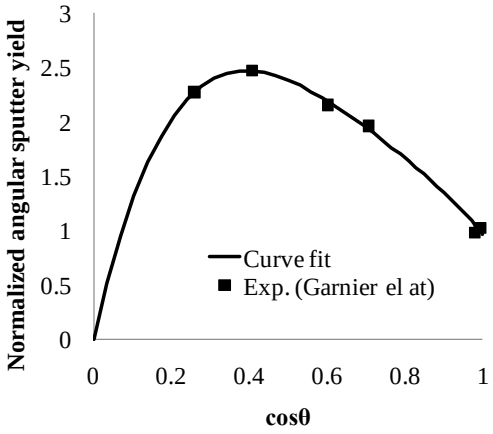


**Figure 7. Angular sputter yield model.**

The specifications are outer channel diameter 62 mm, inner channel diameter 48 mm, and channel length 21 mm.

The magnetic field configuration calculated by FEMM is shown by Fig. 3. The colored square denotes the calculation domain. Note that the calculation domain includes the insulator BN wall region. Cartesian grid in cylindrical coordinate was used for the cell networks.

### E. Boundary Conditions

The boundary conditions for potential calculation are shown by Fig. 5. Colored square shows the calculation domain. For the conservation of charge, the BN wall surface accumulates charge due to particle bombardment or secondary electron emission. The field inside the BN wall was directly solved, and the Neumann condition was imposed at the backside of BN wall. At the same time, Dirichiet condition (experimental data of floating potential) was imposed at the magnetic circuit boundary.

Figure 5 presents the boundary conditions for particles. Electrons are injected from the plume and exit boundary to keep the local quasi-neutrality with 1 eV as initial energy.

### F. Sputter model

The channel wall erosion caused by ion bombardment was evaluated in terms of channel wall reduction rate. The sputtering yield model can be written as

$$Y(E_i, \theta_i) = Y_n(E_i) \times Y_\theta(\theta_i) \tag{12}$$

Where $Y_n(E_i)$ is the sputtering yield as the function of incident ion energy when the incident angle is normal to the wall surface, and $Y_\theta(\theta_i)$ is the normalized angular yield dependence. According to Yamamura and Tawara model,[15] the ion energy dependence of normal sputtering yield can be written as

$$Y_n(E_i) = \frac{AE_i^{0.5}}{1+BE_i^{0.3}}\left(1-\sqrt{\frac{E_{th}}{E_i}}\right)^{2.5} \qquad (13)$$

Where $E_i$ is incident ion energy, $A, B$, and $E_{th}$ are coefficients. Because of the shortage of BN sputtering yield data for low energy xenon ion impact, the coefficients were decided by comparing the erosion rate result of simulation and multilayer coating measurement. Figure 6 shows the normal sputter model used in this study. The coefficients are $A = 1.6543, B = 154.4$, and $E_{th} = 5$ [eV]. Figure 7 presents the angular sputter yield model based on experimental data.[16]

### G. Multilayer Coating Method

Multilayer coating measurement was implemented as the experimental approach. By using small chips with multilayer coating as the sensor of erosion detection, rapid and direct measurement with fine spatial resolution was enabled. These advantages make this method a powerful tool for validation of numerical simulation. Figure 8 shows the schematic of multilayer coating method. Small chip with alternative metal and insulator material coating is inserted into the channel wall, so that the channel recession rate can be measured by the periodic emission of metal layer. The detail of the method is described in the Ref.13.

## III. Results

Table 2 presents the result of discharge parameter. Discharge voltage, Xe mass flow rate, and coil current are input parameters. Coil current 1.5 A corresponds to 24 mT of magnetic flux density at the center of channel exit. The simulation result agrees very well with the experimental result for discharge current, thrust, and thrust efficiency. However, the predicted discharge oscillation amplitude was about 25 % higher than the measured

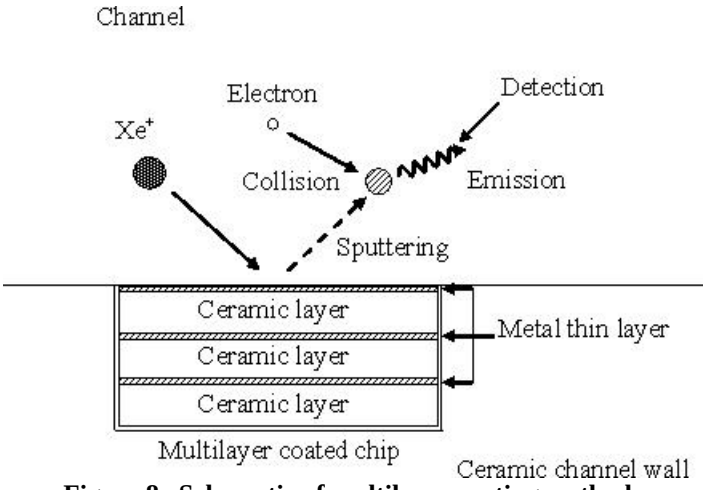


**Figure 8. Schematic of multilayer coating method.**

**Table 2. Discharge parameter.**

| Parameter | Simulation | Experiment |
|---|---|---|
| Discharge Voltage, V | 300 | 300 |
| Mass flow rate, mg/s | 1.36 | 1.36- |
| Coil current, A | 1.5 | 1.5 |
| Discharge current, A | 1.03 | 1.04 |
| Thrust, mN | 15.5 | 15.7 |
| Thrust efficiency, % | 28.7 | 29.4 |
| Discharge oscillation amplitude | 0.29 | 0.23 |

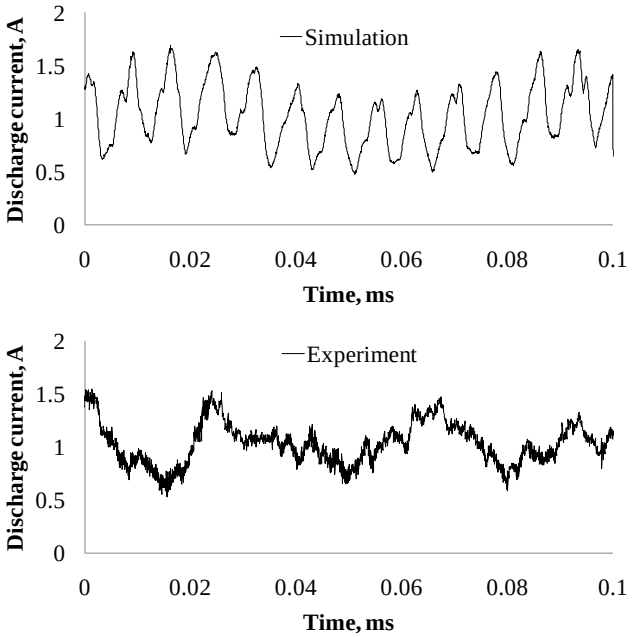


**Figure 9. Discharge current.**

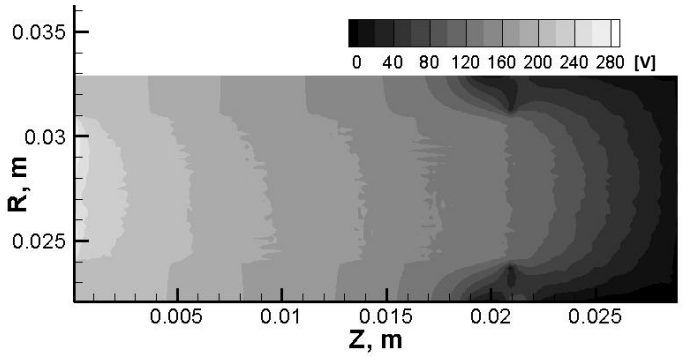


**Figure 9. Plasma potential**

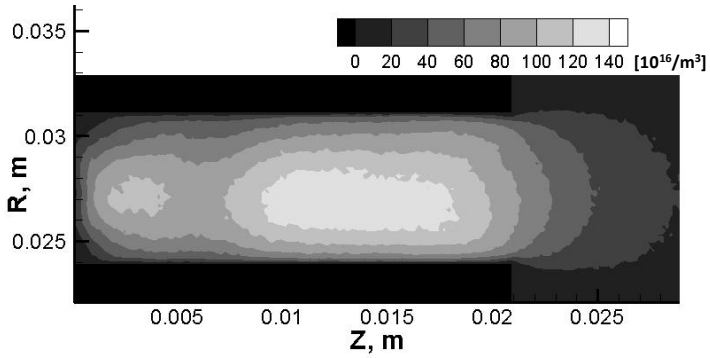


**Figure 10. Electron number density.**

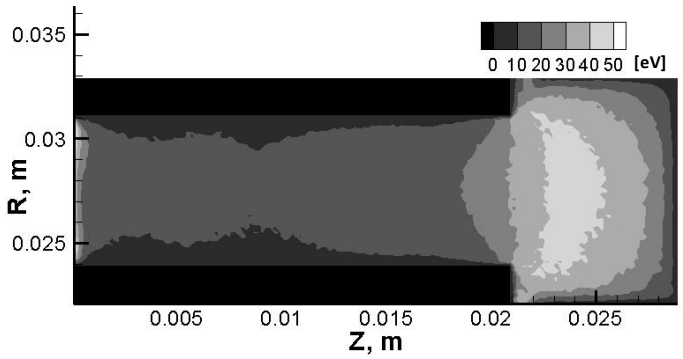


**Figure 11. Electron temperature.**

result. The disagreement of discharge oscillation also can be observed for the discharge current waveform as Fig. 9 shows. The dominant oscillation frequency of discharge current is about 30 kHz for the experiment, whereas it is 15 kHz and 100 kHz for the simulation. The major reason of the disagreement is considered to be the anomalous diffusion model. Parameter tuning of Bohm diffusion coefficient can resolve the problem.

The simulation result of plasma potential, electron number density, and electron temperature are presented by Fig. 9-11, respectively. The results shown are time-averaged over 0.1 ms. The pictures includes 2 mm thick BN wall region, and the channel exit is Z = 0.021 m. Fig. 9 shows that the plasma potential gradually decreases from the anode to the channel exit. There also exits steep radial potential gradient near the channel wall representing the electron repelling wall sheath. The typical potential gap of wall sheath is about 10 V, which is very reasonable compared with the theoretical prediction, or with the result of electron temperature. It is notable that electric field inside the BN wall is not uniform near the channel exit, or the magnetic circuit boundary. This result indicates that imposing simple Neumann condition at the surface of insulator wall without calculating the inside field can lead to wrong result.

Figure 10 shows that the plasma density is high throughout the discharge channel, and takes peak value at the upstream of channel exit. This tendency is caused by the magnetic field configuration of the thruster, which has relatively strong magnetic field throughout the channel as shown by Fig. 3. It is noted that if the picture was not time-averaged, the density peak shifts back and forth in the axial direction because of the ionization oscillation shown by Fig. 9.

The electron temperature presented by Fig. 11 is precisely the averaged electron total kinetic energy. The electron temperature is as high as 30 – 50 eV outside the channel due to the high electric field and low neutral density. However, the temperature is in the vicinity of ionization energy of xenon, which is considered to be reasonable.

The result of channel wall erosion was presented by Fig. 12. The horizontal axis shows the axial position, where 0 mm is the channel exit and -21 mm is the anode. The experimental result was measured by multilayer coating method at the position of -1.5 mm of the outer channel wall. Because the used cylinder sensor chip had the size of 1 mm in diameter, the measurement has 0.5 mm uncertainty of position. The detail of the measurement result is described in Ref. 13. The simulation result presents the channel wall reduction rate distribution throughout the channel. As can be expected from the plasma density distribution, the wall reduction rate is relatively high even at the upstream of the channel. As Fig. 13 shows, the ion wall loss, or the ion flux density impacting the wall is also high throughout the channel and causing the high erosion rate. The ion loss current is as high as 1.23 A in total,

which means that the propellant xenon gas are ionized more than twice in average. This result explains well about the reason of low thrust efficiency presented by Table 2, and indicates that the geometry of the thruster can be largely improved by shortening the channel length.

## IV. Conclusion

In order to develop a lifetime evaluation system without relying on long-time endurance tests, numerical analysis by using Fully Kinetic PIC model and measurement by using Multilayer Coating Method was conducted for a Hall thruster's insulator channel wall erosion. The technique of artificial permittivity was removed from the numerical model by improving the time accuracy and introducing partially implicit method for the field solver. Fine agreements of all discharge parameters except discharge oscillation were obtained between the simulation and experiment result. By coupling with the measurement result of Multilayer Coating Method which compensating for the shortage of low energy sputtering yield data, the profile of channel wall reduction rate was successfully obtained. The result indicates that the efficiency and the lifetime performance of the thruster can be improved by shortening the channel length.

This lifetime evaluation system is potential because the Full Kinetic model provides erosion profile supported by direct wall sheath modeling with acceptable computational cost, and the Multilayer Coating Method enables low-cost and spatial resolved measurement for validation. Further development of the model and application to various situations are expected.

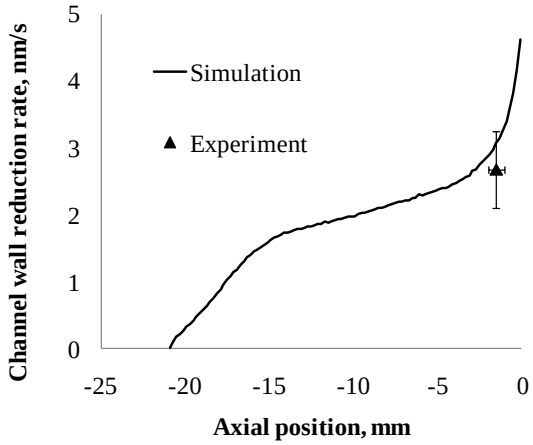


**Figure 12. Channel wall reduction rate**

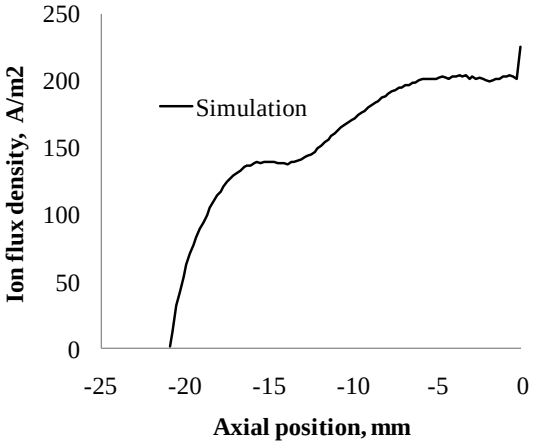


**Figure 13. Ion wall loss**


## Acknowledgments

This work was supported by a Grant-in-Aid for Scientific Research (B), No.21360415, sponsored by the Ministry of Education, Culture, Sports, Science and Technology, Japan.

## References


[1]N. Yamamoto, Lei Tao, Binyamin Rubin, John D. Williams, and Azer P. Yalin, "Sputter Erosion Sensor for Anode Layer-Type Hall Thrusters Using Cavity Ring-Down Spectroscopy," *AIAA Journal of Propulsion and Power 2010*, 0748-4658 Vol.21, No.5 (870-876).

[2]D. Pagnon, M. Touzeau, and P. Lasgorceix, "Control of the Ceramic Erosion by Optical Emission Spectroscopy: Parametric Studies of SPT100-ML," *40th AIAA/ASME/SAE/ASEE Joint Propulsion Conference & Exhibit*, Fort Lauderdale, Florida, AIAA Paper 2004-3773, July 2004.

[3]A. I. Bugrova, A. M. Bishaev, A.V. Desyatskov, M. V. Kozintseva, and M. Prioul, "Spectral Investigation of SPT MAG Insulator Erosion," *29th International Electric Propulsion Conference*, Princeton University, IEPC-2005-167, November 2005.

[4]David, Manzella., John, Yim., and Iain, D. Boyd. "Predicting Hall Thruster Operational Lifetime," *40th AIAA/ASME/SAE/ASEE Joint Propulsion Conference & Exhibit*, Fort Lauderdale, Florida, AIAA Paper 2004-3953, July 2004.

[5]Shannon, Y. Cheng., and Manuel, Martinez-Sanchez. "Hybrid Particle-in-cell Erosion Modeling of Two Hall Thrusters," AIAA *Journal of Propulsion and Power 2008*, Vol.24, No.5 pp.987-998.

[6]Ioannis, G. Mikellides., Ira, Katz., Richard, R. Hofer., Dan, M. Goeble., Kristi, de, Grys., and Alex, Mathers. "Magnetic Shielding of the Acceleration Channel Walls in a Long-Life Hall Thruster," *46th AIAA/ASME/SAE/ASEE Joint Propulsion Conference & Exhibit*, Nashville, TN, AIAA Paper 2010-6942, July 2010.

[7]Kristi de Grys, Alex Mathers, Ben Welander, and Vadim Khayms, "Demonstration of 10,400 Hours of Operation on a 4.5 kW Qualification Model Hall Thruster," *46th AIAA/ASME/SAE/ASEE Joint Propulsion Conference & Exhibit*, Nashville, TN, AIAA Paper 2010-6698, July 2010.

[8]V. A. Petrosov, A. I. Vasin, V. I. Baranov, J. R. Wetch, E. J. Britt, S. P. Wong, and R. Lin, "A 2000 Hours Lifetime Test Results of 1.3 kW T-100 Electric Thruster," *24th International Electric Propulsion Conference*, Moscow, IEPC-95-41

[9]C. E. Garner, J. R. Brophy, J. E. Polk and L. C. Pless, "A 5,730-Hr Cyclic Endurance Test of the SPT-100," *31st AIAA/ASME/SAE/ASEE Joint Propulsion Conference & Exhibit*, San Diego, CA, AIAA Paper 1995-2667, July 1995.

[10]Justin, Fox., Alla, Batishcheva., Oleg, Batishchev., and Manuel, Martinez-Sanchez. "Adaptively Meshed Fully-Kinetic PIC-Vlasov Model For Near Vacuum Hall Thrusters," *42th AIAA/ASME/SAE/ASEE Joint Propulsion Conference & Exhibit*, Sacramento, California, AIAA Paper 2006-4324, July 2006.

[11]Shigeru, Yokota., Kimiya, Komurasaki., and Yoshihiro, Arakawa. "Plasma Density Fluctuation Inside a Hollow Anode in an Anode-layer Hall Thruster," *42th AIAA/ASME/SAE/ASEE Joint Propulsion Conference & Exhibit*, Sacramento, California, AIAA Paper 2006-5170, July 2006.

[12]Rodney J. Mason, "Implicit Moment Particle Simulation of Plasmas," *Journal of Computational Physics*, Cambridge, Vol. 41, pp 233-244, 1981.

[13]Shinatora, Cho., Shigeru, Yokota., Kentaro, Hara., Daisuke, Takahashi., Yoshihiro, Arakawa., and Kimiya, Komurasaki. "Hall Thruster Channel Wall Erosion Rate Measurement Method Using Multilayer Coating Chip," *46th AIAA/ASME/SAE/ASEE Joint Propulsion Conference & Exhibit*, Nashville, TN, AIAA Paper 2010-6697, July 2010.

[14]Naoji, Yamamoto., Kimiya, Komurasaki., and Yoshihiro, Arakawa. "Discharge Current Oscillation in Hall Thrusters," *AIAA Journal of Propulsion and Power 2005*, vol.21 no.5, pp.870-876.

[15]Yamamura, Y., and Tawara, H. "Energy Dependence of Ion-Induced Sputtering Yields from Monatomic Solids at Normal Incidence," *Atomic Data and Nuclear Data Tables*, Vol. 62, No. 2, March 1996, pp.149-253

[16]Garnier, Y., Viel, V., Roussel, J.-F., and Bernard, J. "Low-energy Xenon Ion Sputtering of Ceramics Investigated for Stationary Plasma Thrusters," *Journal of Vacuum Science and Technology A*, Vol. 17, No. 6, Nov/Dec 1999, pp.3246-3254